Hindawi
Advances in Materials Science and Engineering
Volume 2018, Article ID 6514025, 13 pages
https://doi.org/10.1155/2018/6514025

Research Article

Experimental and Numerical Investigation of Concrete-Filled Double-Skin Steel Tubular Column for Steel Beam Joints

Dongfang Zhang,[1] **Junhai Zhao**,[1] **and Yufen Zhang**[2]

[1]*School of Civil Engineering, Chang'an University, Xi'an, Shaanxi 710061, China*
[2]*School of Civil and Transportation Engineering, Hebei University of Technology, Tianjin 300401, China*

Correspondence should be addressed to Dongfang Zhang; zhangdongfang_2008@163.com

Received 28 February 2018; Accepted 17 July 2018; Published 5 August 2018

Academic Editor: Nadezda Stevulova

This paper presents a new type of joint for connecting steel beams with a concrete-filled double-skin steel tubular (CFDST) column. Four half-scale specimens of the joint with different specifications were constructed and tested under a constant axially compressive force with vertical low-reversal loads applied to the beam ends to examine their failure modes and hysteretic behaviors. The beam hinging mechanism of the joint was observed in the radian area of the horizontal end plates. The proposed connection was found to exhibit good energy dissipation capabilities with its limit rotation in the failure state reaching 0.05 rad, thus satisfying the FEMA-350 ductility requirement of ≥0.03 rad for seismic resistance. A finite element analysis (FEA) model of the joint was also established and validated by comparing its predictions with experimental results. The FEA model was used to investigate the effects of different parameters such as the stiffened height of the web anchorage plate, axial load level, steel and concrete strengths, steel ratio on the moment-rotation relationship, and initial stiffness of the connection. This paper presents some important design considerations of the connection, as well as aspects requiring further study.

1. Introduction

Concrete-filled steel tubular (CFST) columns exhibit excellent static behavior and seismic resistance and are widely used in construction projects in seismic areas. A recently developed type of CFST column referred to as a concrete-filled double-skin steel tubular (CFDST) column has attracted much attention in the civil engineering community in recent times. A CFDST column is composed of double concentric steel tubes with the internal space fully or partly filled with concrete. Comparing with the conventional CFST column, the bending stiffness, ductility, and seismic performance of the CFDST column are significantly increased because of the inner steel tube [1–4]. CFDST columns may also be effective for dealing with the requirement for large-profile columns in some engineering projects. When used in buildings, CFDST columns are usually connected to steel beams. There have, however, been few studies on such connections, which tend to be complex owing to the double-skin tubes. This, as well as the nonexistence of applicable standard codes and practices, has hampered the application of CFDST columns in high-rise buildings in seismic regions.

There have been previous experimental and numerical studies on the connection of ordinary CFST column to steel beams. Through experiments and simulations, Han and Li [5, 6] investigated the seismic performance of connections between CFST columns and steel beams with external diaphragms. Both the beam and column failures were observed, and a series of numerical parametric investigations were also used to examine the effects of the joint parameters on the initial stiffness, bending capacity, and failure modes of the joints. Jianguo et al. [7] conducted experimental and numerical analyses of the seismic behavior of composite frames with concrete-filled rectangular steel tubular columns (CFRSTCs). The results obtained by an FEA model fitted well with those of model tests in terms of the stiffness, strength, hysteretic behavior, and component deformation. Wang and Spencer [8] experimentally and numerically

investigated a blind bolted end plate joint between a CFST column and a steel beam. Parametric analyses based on a finite element analysis (FEA) model validated by experimental results were used to investigate the behavior of the joint. Based on the findings, they recommended a reasonable bolt anchorage length ratio for this type of joint. Kang et al. [9] numerically investigated the shear bearing capacity of the connection between an internal diaphragm and a concrete-filled steel tube (CFT) column. Based on their findings and previous theory, they proposed relationships between the shear force and the deformation of the modified joint. Rezaifar and Younesi [10] developed a new connection between a CFST column and a steel beam using trapezoidal external stiffeners and horizontal bar mats, and used FEA to investigate its seismic performance. The results indicated that the connection was potentially applicable to constructions in seismic areas, affording a good alternative for connection using continuity plates. Through experiments and simulations, Tao et al. [11] investigated the seismic behavior of the connection between a steel beam and a CFST column using high strength through column bolts and extended end plates. The effects of the yield stress and thickness of the end plate on the rotation stiffness and moment capacity of the joint were examined for integration of the joint in engineering designs. Liu et al. [12] experimentally and numerically investigated the seismic behavior of the connection between a specially shaped CFST column and a steel beam joint. They introduced an exterior diaphragm and a vertical rib as joint stiffeners and analyzed the failure mode, stiffness, and seismic performance index based on the load deformation and strain curves. They proposed a shear resistance formula of the joint based on the internal load transmission for engineering application.

However, there has been very little recent research on the connection of a CFDST column. Zhang et al. [13, 14] presented a ring beam joint between a CFDST column and reinforced concrete (RC) beams. Experimental and numerical analyses were used to investigate the seismic behavior of the joint. Nevertheless, to enable broad application of the CFDST column, it is necessary to design a joint for connecting it to a steel beam. Zhang et al. [15] proposed a joint for connecting a CFDST column to a steel beam based on the idea of the vertical stiffener joint. Experiments were performed to evaluate the seismic behavior of the joint, which was found to exhibit high strength, stiffness, ductility, and energy dissipation capability.

In the present study, the mechanical behavior of a progressive joint for connecting a CFDST column to a steel beam was investigated experimentally and numerically. An experimental program for investigating the composite joint was first developed. An FEA model of the joint was subsequently established, taking into consideration the concrete confinement effect, concrete damage characteristic, and interaction between the concrete and the steel tube. The FEA model was validated by comparing its predictions with the experimental results. A parametric analysis based on the FEA model was also conducted to investigate the effects of different parameters such as the stiffness height, axial load level, material strength, and steel ratio on the joint behavior.

2. Experimental Program

2.1. Design of Test Specimens. The prototypes of the steel beam and the CFDST column of the test specimens were designed in accordance with GB 50936-2014 [16]. To achieve an excellent behavior of the CFDST column, a web anchorage plate was attached to the inner steel tube for connection to the steel beam through the outer steel tube, as shown in Figure 1. A horizontal end plate with a reduced section was also welded to the outer tube wall and the web anchorage plate, for welding to the flange of the steel beam. Finally, a vertical plate was welded around the connection region to strengthen the stability of the composite joint. The detailed construction information and parameters of the tested joint specimens are presented in Figure 2 and Table 1, respectively.

The section of each column consisted of an outer square tube and an inner circular tube of seamless steel, with the internal space filled with concrete, as shown in Figure 3(a). The section of the square tube measured $250 \times 250 \times 8$ mm (side length × side length × thickness), and that of the circular tube measured 133×6 mm (diameter × thickness). The H-shaped section of each steel beam measured $244 \times 175 \times 7 \times 11$ mm (height × flange width × web thickness × flange thickness), as shown in Figure 3(b). The size of the horizontal end plate is shown in Figure 3(c). The main parameters of the composite joint included the type of the two web anchorage plates and the extension length of the vertical plate, as shown in Figures 3 (d)–3(f).

2.2. Test Setup and Loading Program. The purpose of the experimental study was to simulate the mechanical properties of the tested joints under earthquake action. The boundary conditions of a model of the cruciform beam-to-column joint were reproduced in the test setup, as shown in Figure 4(a). A 2000 kN vertical hydraulic jack was placed at the top of the column and used to apply a constant vertical force to simulate the effect of the upper floors of a multistorey building. The vertical actuator was glidingly attached to the reaction frame, and a spherical hinge was placed between the actuator and the column to simulate the inflection point of the joint specimen. The column end was restrained by a rigid transverse beam connected to the reaction wall, but allowed to freely rotate in the loading plane. A vertical low-reversal cyclic load was applied to each end of the beam by an MTS hydraulic actuator to simulate the seismic loading effect. Four specially designed out-of-plane lateral braces were used to avoid torsion of the joint specimen during the loading process, as shown in Figure 4(b).

During the test of all the specimens, after calibration of all the instrumentation, the vertical hydraulic jack was first used to apply a constant axial load of 1514 kN to the top of the column. A vertical low-reversal load was then applied to each end of the two-segment beam under displacement control, as depicted in Figure 5. The loading profile in the figure is based on the recommendations of the Chinese standard JGJ/T 101-2015 [17]. For convenience of description of the testing process, the pushing and pulling

actions of the vertical actuator of the right beam segment were defined as positive (+) and negative (−), respectively. The loading process began with one cycle of each of ±6, ±12, and ±18 lateral displacements. Subsequently, sets of three cycles with progressively increasing lateral displacement amplitudes of ±24, ±30, ±36, ±42, ... were implemented until failure of the specimen or reduction of the load below 85%.

2.3. Material Properties. The strength and elastic modulus of the steel were measured in accordance with the GB/T 228.1-2010 standard [18]. The same type of steel was used to fabricate the web anchorage plates and the outer square tubes, whereas another type was used to fabricate the horizontal end plates and vertical plates. The detailed mechanical properties of all the steel components are presented in Table 2. Nine concrete cubes with a side length of 150 mm were molded and their compressive strength was measured using the standard test method. The average compressive strength f_{cu} was determined to be 59.5 MPa.

3. Finite Element Modelling

The finite element program ABAQUS was used to conduct some pertinent parametric investigations on the tested composite joint. The principal modelling factors of the joint included the element types, meshes, connections between elements, material models, boundary conditions, and calculation method.

3.1. Element Types and Meshes. The steel and concrete components were modeled by solid elements (C3D8R) of an eight-node reduction integral format in ABAQUS/CAE 6.11. The calculation precision is even more precise when the grid is distorted. In addition, under a bending moment, the occurrence probability of the shear self-locking phenomenon is low. The calculation can still be continued with relative accuracy under a larger model deformation.

The structured adaptive grid meshing technique was used to achieve an appropriate element shape. A relatively fine mesh was applied to the core concrete and steel beam because of their complex stress distribution and obvious deformation. The FEA model of the SBJ2-2 specimen is shown in Figure 6.

3.2. Material Models

3.2.1. Material Modelling of Steel. A nonlinear combined (isotropic/kinematic) hardening plasticity model was applied to the steel components including the steel tubes, steel beams, and all the construction plates of the joint model. The well-known Bauschinger effect under cyclic loading was considered in the steel model.

The multilinear stress-strain relationship model presented by Abdel-Rahman and Sivakumaran [19] was applied to the square and circular steel tubes to approximate the real performance of steel tubes under seismic action. A square steel tube section in the model was divided into the corner zone and the flat zone, as shown in Figure 7. The stress-stain relationship of the flat zone was also applied to the circular steel tube in the analysis. The equation of the five stages of the elastic-plastic stress-strain model is available in [20].

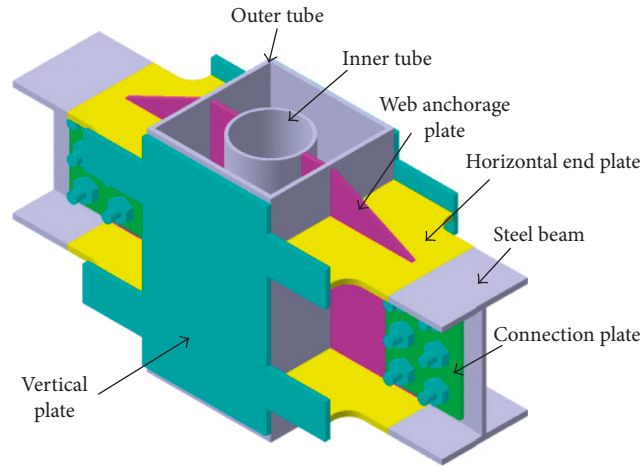

Figure 1: Construction of joint specimen.

A trilinear stress-strain elastic-plastic model was applied to the steel beams, construction plates, and bolts for better simulation of the descending branch of the force-deformation curve of the joint model under cyclic loading. The three stages of the constitutive model are shown in Figure 8, where $\varepsilon_A = f_y/E_s$, $\varepsilon_B = (f_u - f_y)/0.1E_s$, $\varepsilon_C = 0.03$, and f_y, f_u, and E_s are listed in Table 2.

3.2.2. Material Modelling of Concrete. Concrete is a discrete material and more complex than steel. A concrete damage plasticity (CDP) model was applied to the concrete in the present analysis. The model is based on an elastic-plastic model, includes the damage variable factor D, and well simulates the stiffness degradations of concrete under cyclic loading, according to Lubliner et al. [21] and Lee and Fenves [22]. Under axial loading, the core concrete was subjected to the double-side constraints of the internal and external steel tubes. Owing to the interactions between the steel tubes and the concrete, the mechanical properties of the core concrete were more complex than usual. The confined concrete stress-strain relationship proposed by Han et al. [23] was used to analyze the core concrete of the CFST in compression, while the core concrete constitutive model was applied to the tensile state in accordance with the Chinese code GB 50010-2010 [24]. The compressive stress-strain curves are shown in Figure 9.

The parameters of the CDP model included a dilation angle of 30°, plastic potential eccentricity of 0.1, ratio of the ultimate compressive strength to the biaxial compressive strength of 1.16, ratio between the second stress invariants on the meridional plane and the compression meridian of 2/3, and viscosity coefficient of 0.0005. There is no stipulated method for determining the damage variable factor (D) in the relevant standards and regulations. The following equation is used to determine the compression damage factor d_c and the tension damage factor d_t [25]:

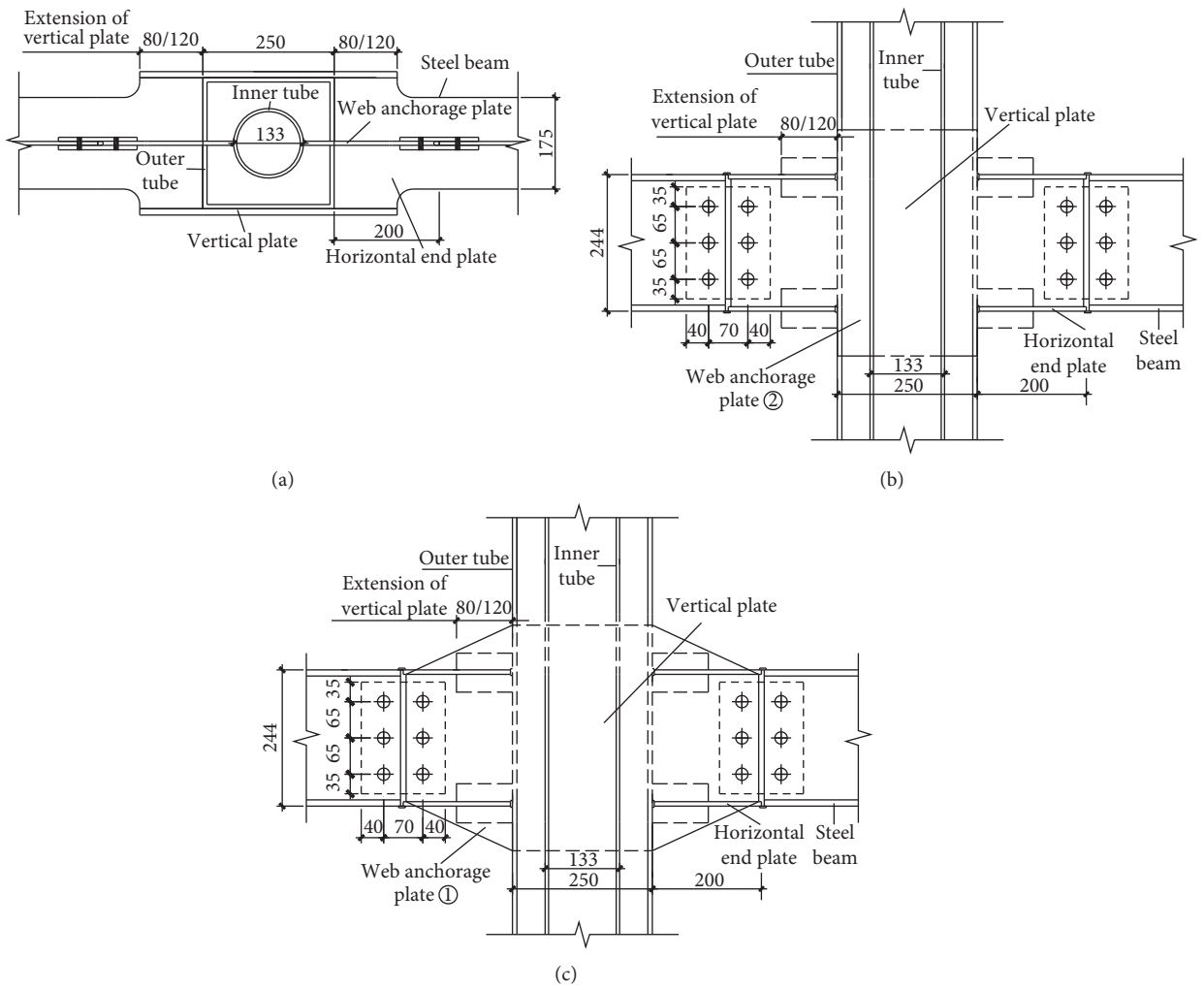

Figure 2: Details of the joint specimens. (a) Plan view of a specimen. (b) Elevation view of the SBJ1-1 and SBJ1-2 specimens. (c) Elevation view of the SBJ2-1 and SBJ2-2 specimens.

$$d_k = \frac{(1-\beta)\varepsilon^{\text{in}} E_c}{\sigma_k + (1-\beta)\varepsilon^{\text{in}} E_c} \quad (k = t, c), \tag{1}$$

where the subscript k ($k = t, c$) represents the tensile or compressive stress state, β is the ratio of the plastic strain to the inelastic strain (β is within 0.35–0.7 when the concrete is in the compressive state and 0.50–0.95 when in the tensile state), ε^{in} is the inelastic strain of the concrete (given by (2)), σ_k ($k = t, c$) is the tensile or compressive stress of the concrete corresponding to the strain ε, and E_c is the elastic modulus of the concrete (3.6×10^4 MPa according to GB 50010-2010) [24].

$$\varepsilon^{\text{in}} = \varepsilon - \sigma_k E_c^{-1}. \tag{2}$$

3.3. Interaction between Concrete and Steel Tubes. The contact relationship between the steel tubes and the concrete was defined by considering the slippages in the normal and tangential directions on the surfaces of the two materials. The contacting surfaces were allowed to transfer the pressure in the tangential direction, but penetration in the normal direction was not allowed. Hard contact was applied in the normal direction to simulate the surfaces of the steel tubes and core concrete, while the Mohr–Coulomb friction model was applied in the tangential direction. In the present analysis, the friction coefficient in the tangential direction was considered to be 0.25 in accordance with [26]. The tangential bond shear stresses between the surfaces of the steel tubes and the concrete were as detailed by Roeder et al. [27].

Table 1: Details of the test specimens.

Specimen	Web anchorage plate	Extension of vertical plate
SBJ1-1	Nonstiffening	80 mm
SBJ1-2	Nonstiffening	120 mm
SBJ2-1	Stiffening	80 mm
SBJ2-2	Stiffening	120 mm

3.4. Finite Element Model Description. The FEA model of the representative SBJ2-2 specimen is illustrated in Figure 6. The model considers the material and geometric nonlinearities

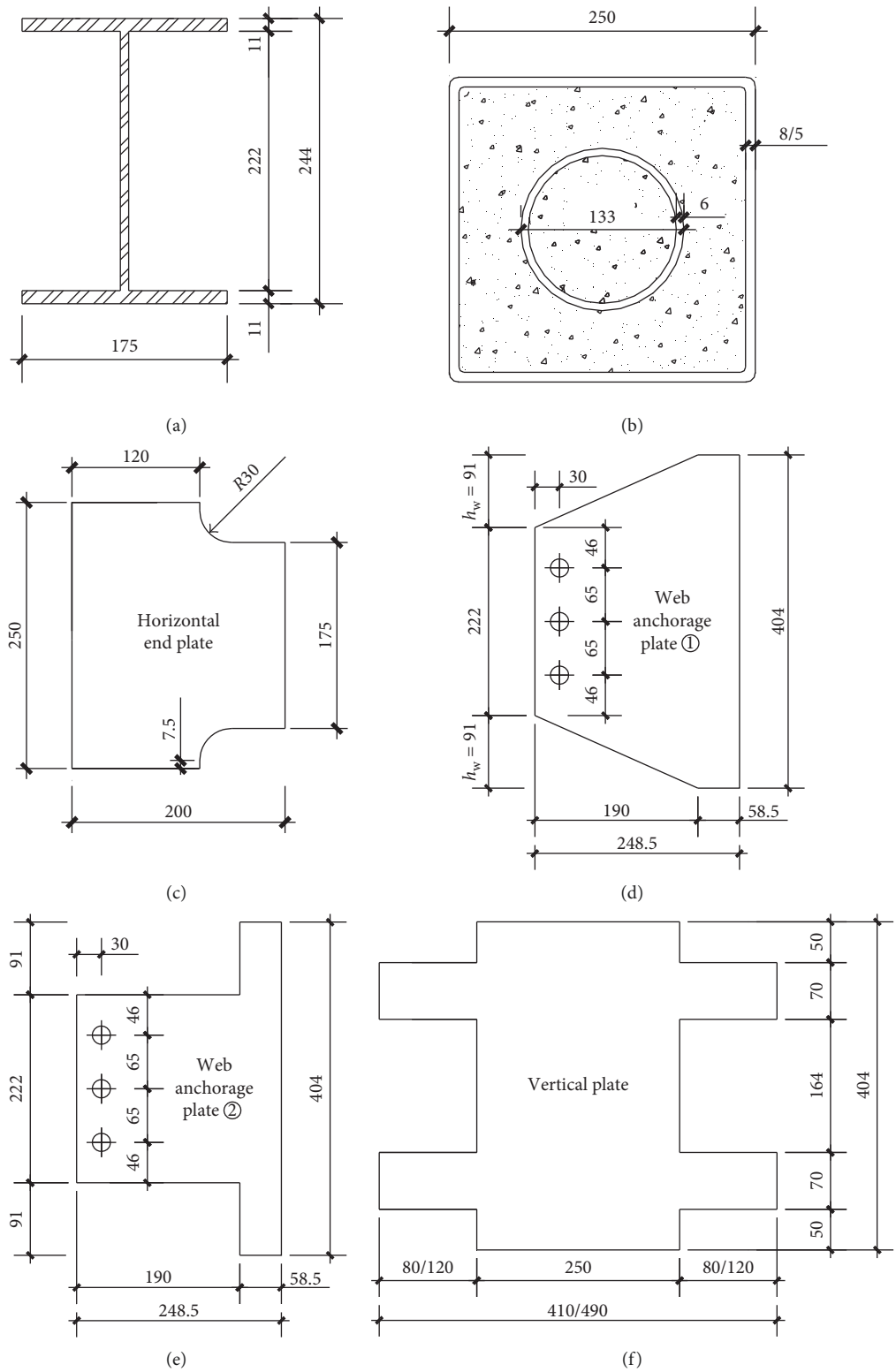

Figure 3: Details of the beam, column, and construction plates. (a) Beam. (b) Column. (c) Horizontal end plate. (d) Stiffening type. (e) Nonstiffening type. (f) Vertical plate.

and the boundary conditions. Two reference points were established on the top and bottom of the column, respectively. The test boundary conditions were reproduced in the FEA model. An axial load N_0 was applied to the top of the CFDST column in the first step, and a cyclic displacement load was subsequently applied to the beam trips. The Newton–Raphson method in the ABAQUS/Standard implicit calculation module was used to solve the model.

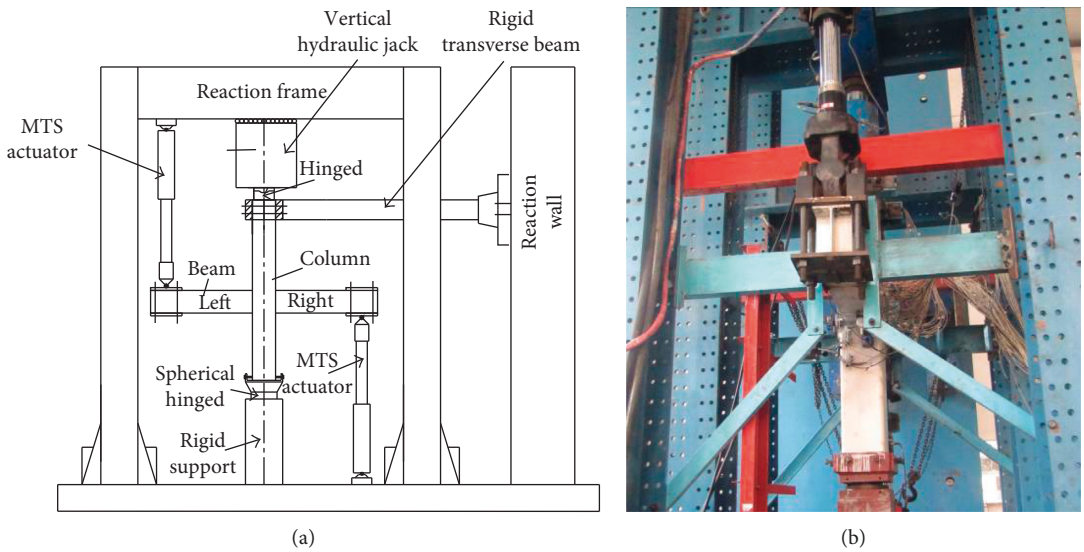

Figure 4: Test setup. (a) Diagram of the loading device. (b) Lateral brace of the steel beams.

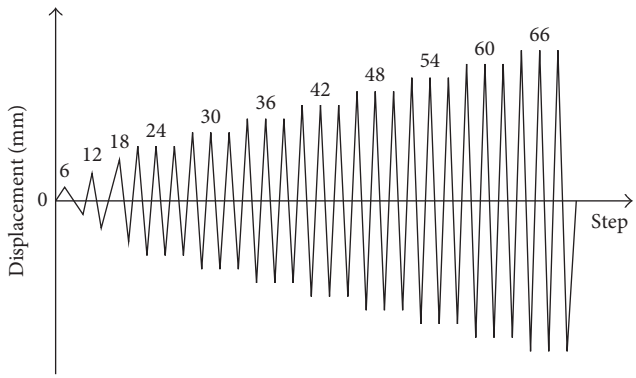

Figure 5: Loading history.

3.5. Verification

3.5.1. Failure Mode. Figures 10–13 compare the failure modes determined by tests and FEAs, from which rough agreement can be observed. The indicated large deformation of the steel is approximatively attributed to fracturing. The radian areas of the horizontal end plates of both the left and right segments of the beam of the SBJ1-1 specimen tore during the test, as shown in Figures 10(a) and 10(c), respectively, and the FEA results reveal obvious buckling at the same locations, as can be observed from Figure 10(b). The two results are thus in good agreement. In contrast to the SBJ1-1 specimen with the extension 80 mm of the vertical plate, the extension length of the vertical plate in the SBJ1-2 specimen was 120 mm. The failure positions in the latter specimen observed in the test and simulation were away from the joint core region, as shown in Figure 11. Conversely, the SBJ2-1 specimen with extension 80 mm failed starting from the break at the radians of the horizontal end plate, with slight buckling of its stiffening web anchorage plate observed in both the test and simulation results, causing a small fracture of the steel tube wall, as shown in Figure 12. Comparing with the SBJ2-1 specimen, the phenomenon of fracture on the steel tube did not happen for the SBJ2-2 specimen with extension 120 mm, as shown in Figure 13. The test and simulation results for the SBJ2-2 specimen indicated that the plastic hinge obviously moved away from the steel tube face due to the longer extension length of the vertical plate.

The failure modes of a composite joint are affected by the formation of the web anchorage plate and the extension length of the vertical plate. The joint construction details can be modified to adjust the beam failure modes to satisfy the design requirements of "strong column, weak beam" and "strong joint, weak component" for seismic resistance.

3.5.2. Moment-Rotation Hysteresis Curves. The hysteresis curve is an important indication of the seismic performance of a structure. The moment-rotation (M-θ) hysteresis curves of the different specimens of the considered composite joint are shown in Figure 14. Generally, good agreement can be observed between the M-θ hysteresis curves obtained from the test and FEA results, with the pinching phenomenon particularly well reproduced by the FEA model. The reloading and unloading stiffness predicted by FEA are also close to those determined by testing. The real mechanical behavior of the joint can thus be investigated using the present FEA model. However, the numerical simulation results are not entirely consistent with those of the tests. This is mainly because of the double stress complexity factors in the heat zone generated by the welding of the steel and the differing weld qualities, which cannot be precisely simulated by the FEA model.

Figure 14 shows that the composite joint has a shuttle-shaped hysteresis curve and possesses good energy dissipation capabilities, as indicated by the area of the envelope. The limit rotation of the joint also reaches 0.05 rad in the failure state, satisfying the FEMA-350 ductility requirement of no less than 0.03 rad for seismic resistance [28].

Table 2: Material properties of the steel components.

Item	Thickness t (mm)	Yield strength f_y (MPa)	Tensile strength f_u (MPa)	Elastic modulus E_s (MPa)
Square tube	8	338.12	481.70	2.27×10^5
Circular tube	6	323.08	491.39	2.19×10^5
Beam flange	11	272.41	447.40	2.23×10^5
Beam web	7	291.00	457.23	2.22×10^5
Horizontal end plate	12	272.61	445.86	2.18×10^5

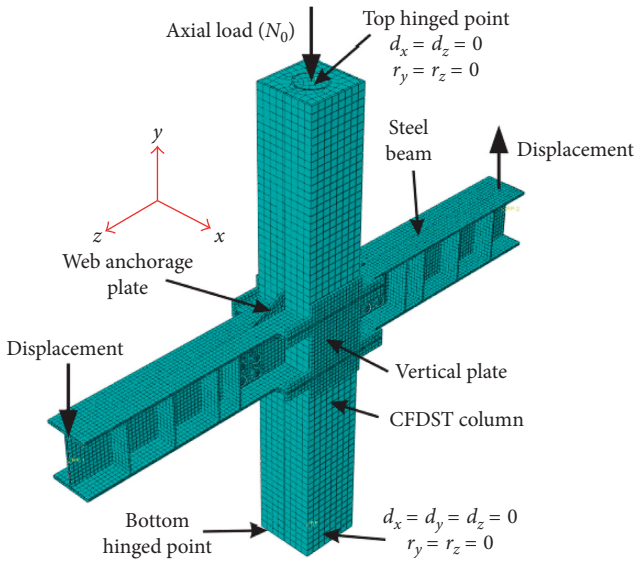

Figure 6: General view of the FEA model of the SBJ2-2 specimen.

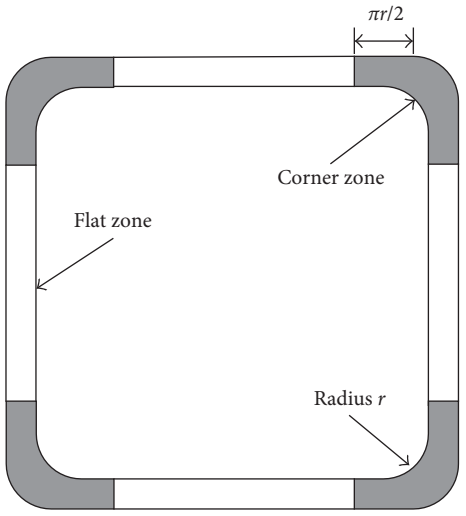

Figure 7: Flat and corner zones of the section of a cold-formed square steel tube.

The forgoing shows that the failure pattern, hysteresis curve, bearing capacity, and stiffness predicted by the FEA model are in good agreement with the test results. The FEA model thus adequately simulates the nonlinear mechanical properties of the composite joint and can be used for further parametric analysis.

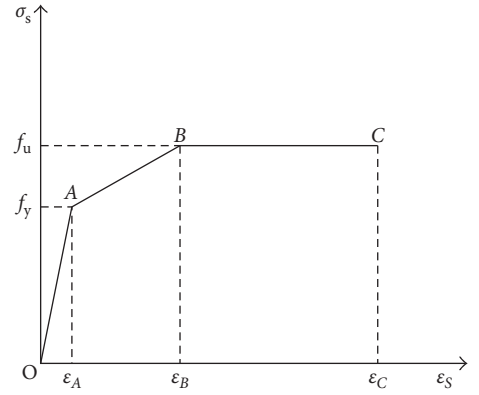

Figure 8: Constitutive trilinear stress-strain relationship.

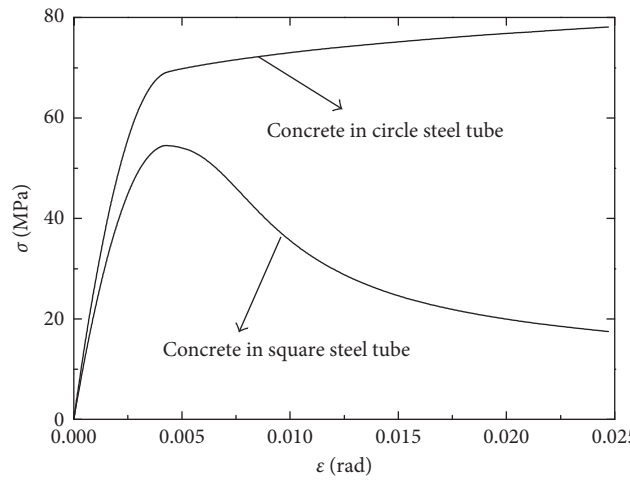

Figure 9: Compressive stress-strain curves of the core concrete.

4. Parametric Investigation

The proposed FEA model was used to conduct a parametric investigation to determine the effects of the joint parameters on its moment-rotation relationship. The main parameters included the height of the stiffening of the web anchorage plate (h_w), axial load level (n), material strength, steel ratio of the column (α), beam-to-column linear stiffness ratio (k_i), and beam-to-column bending capacity ratio (k_m).

The axial load level (n) was defined in this study as N_0/N_u, where N_0 and N_u are, respectively, the axial load applied to the CFDST column and the compressive bearing capacity of the

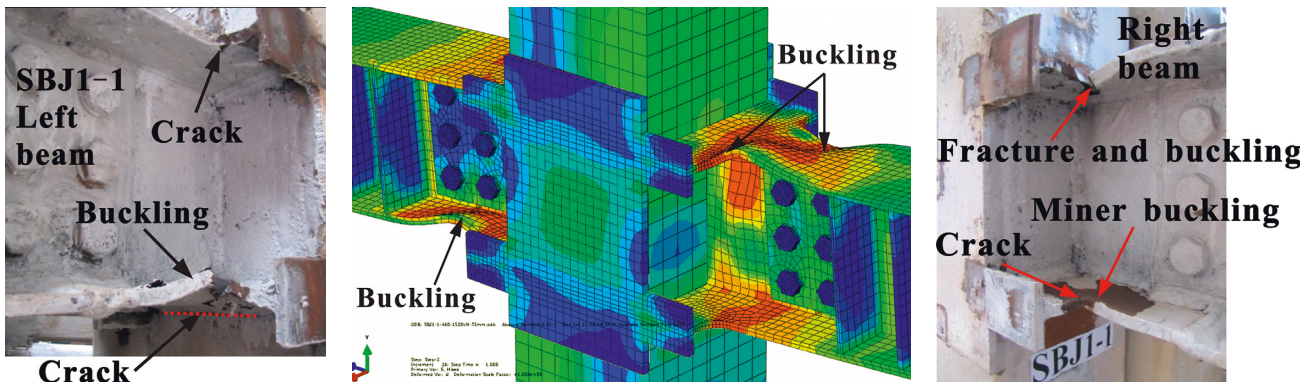

(a) (b) (c)

Figure 10: Comparison of the failure modes of the SBJ1-1 specimen determined by test and FEA. (a) Test: left beam segment. (b) FEA. (c) Test: right beam segment.

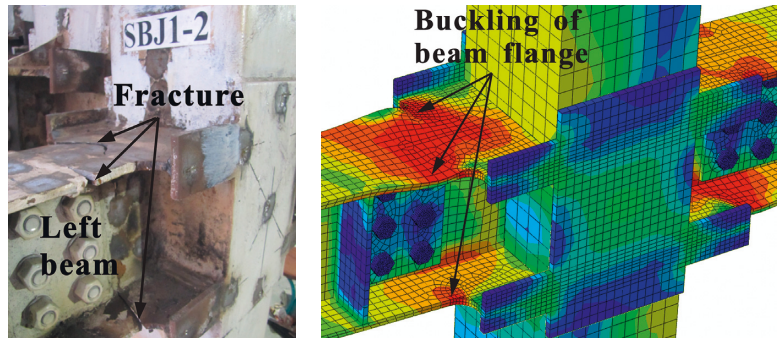

(a) (b)

Figure 11: Comparison of the failure modes of the SBJ1-2 specimen determined by test and FEA. (a) Test. (b) FEA.

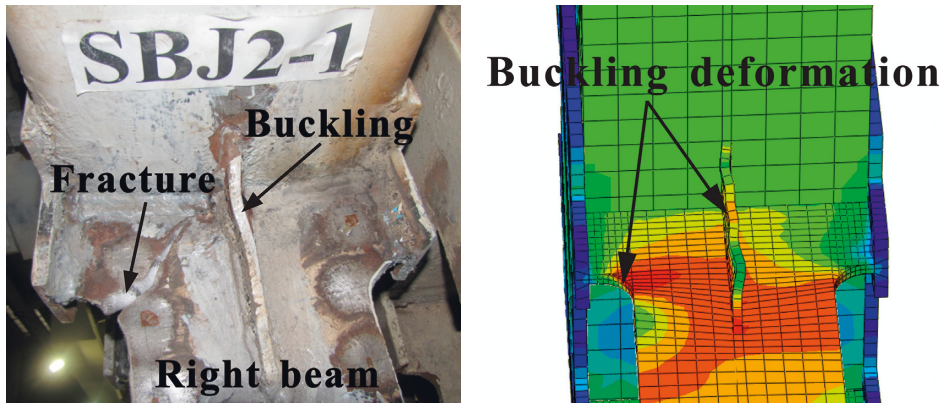

(a) (b)

Figure 12: Comparison of the failure modes of the SBJ2-1 specimen determined by test and FEA. (a) Test. (b) FEA.

CFDST column, as calculated by Zhang et al. [29]. The steel ratio of the column (α) was defined as A_s/A_c, where A_s and A_c are, respectively, the cross-sectional areas of steel tubes and the concrete filled into the column. The beam-to-column linear stiffness ratio (k_i) was defined as i_b/i_c, where i_b and i_c are, respectively, the linear stiffness of the steel beam and the CFDST column. The beam-to-column bending capacity ratio (k_m) was defined as M_b/M_c, where M_b and M_c are, respectively, the bending capacities of the steel beam and the CFDST column calculated according to CECS 159: 2004 [30].

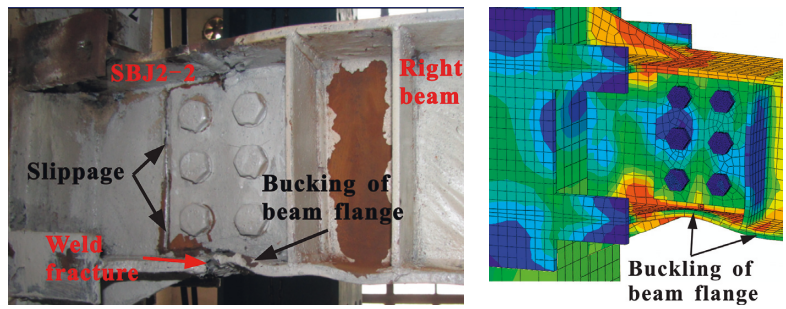

Figure 13: Comparison of the failure modes of the SBJ2-2 specimen determined by test and FEA. (a) Test. (b) FEA.

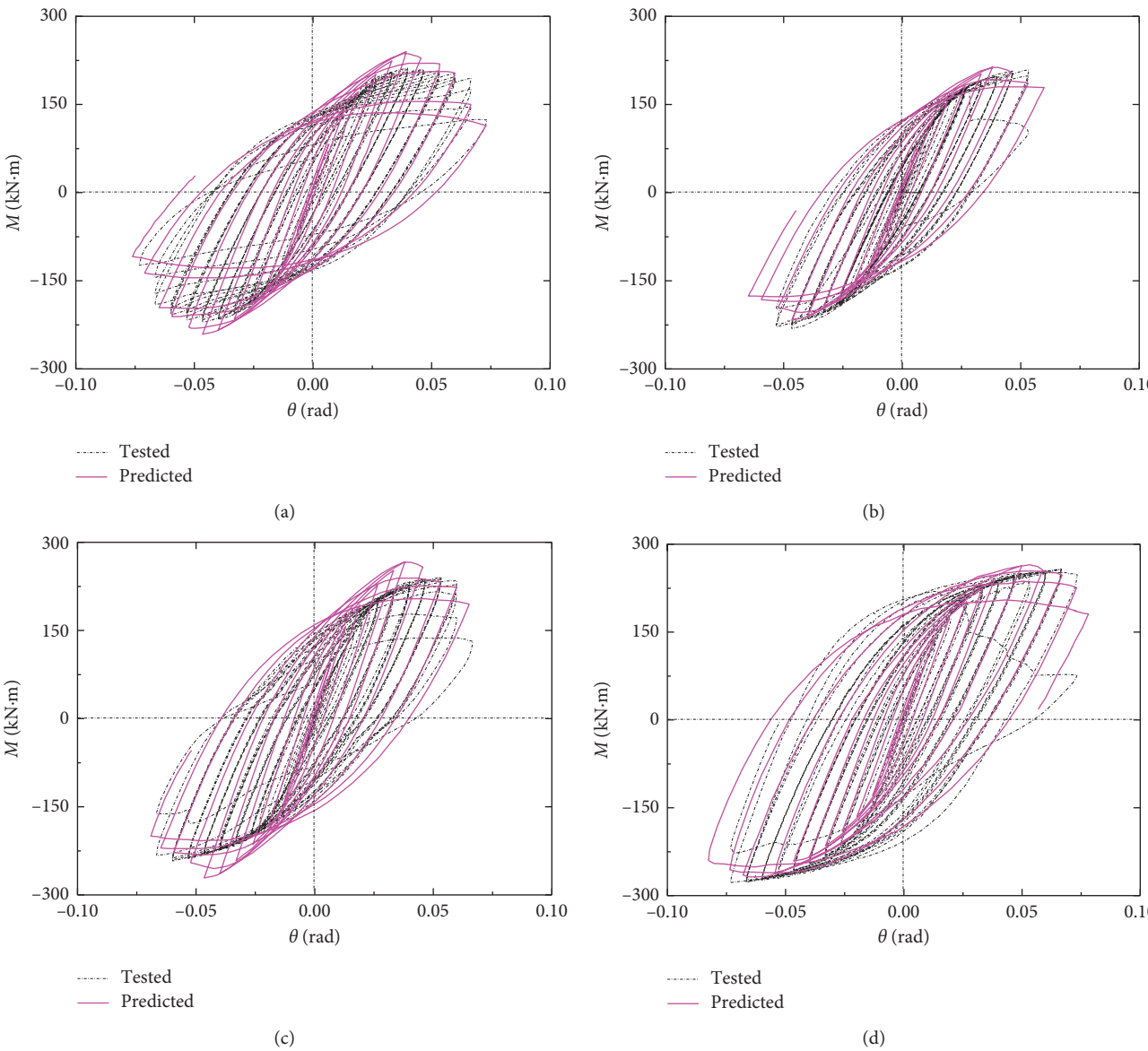

Figure 14: Comparison of the hysteresis curves obtained from the test and FEA results. (a) SBJ1-1. (b) SBJ1-2. (c) SBJ2-1. (d) SBJ2-2.

The basic parameter values used for the calculation examples are as follows:

(i) Joint type: cruciform joint with stiffening of the web anchorage plate, $h_w = 100$ mm

(ii) CFDST column: section as shown in Figure 3(a), height = 2.1 m, $f_y = 345$ MPa, $f_{cu} = 60$ MPa, and $N_0 = 2633$ kN ($n = 0.4$)

(iii) Steel beam: H-244 × 175 × 7 × 11 mm, span length- = 2.5 m, and $f_y = 345$ MPa

(iv) Other parameters: $\alpha = 0.194$, $k_i = 0.434$, and $k_m = 0.592$.

4.1. Effect of Stiffened Height of Web Anchorage Plate (h_w). The effect of the stiffened height was investigated by varying its value as $h_w = 0$, 40, 80, and 100 mm. Figure 15(a) shows the effect on the M-θ relationship of the composite joint. It can be observed that the initial stiffness and ultimate bending capacity of the joint are enhanced with increasing stiffened height (h_w). The stiffened height of the web anchorage plate (h_w) is evidently an important determinant of the M-θ relationship of the considered composite joint. In addition, a stiffened height of 100 mm can be observed to optimize the behavior of the joint for the sizes of the beam and column in the present example. In practical engineering applications, the space utilization rate of a building structure is affected by the stiffened height of the web anchorage plate (h_w).

4.2. Effect of Column Axial Load Level (n). Figure 15(b) shows the effect of the column axial load level (n) on the M-θ relationship, as n is varied as 0, 0.2, 0.4, 0.6, and 0.8. It can be seen that the ultimate bending capacity is only slightly affected by the variation, whereas the initial stiffness is significantly enhanced with increasing n. The composite joint thus exhibits a good bearing capacity under a high axial load level, as well as under a high axial compression ratio ($n = 0.6$; $N_0 = 3950$ kN).

4.3. Effect of Strength of Steel Beam (f_{y1}). The effect of the strength of the steel beam (f_{y1}) on the M-θ relationship was investigated by varying f_{y1} as 235, 345, 390, and 420 MPa, as shown in Figure 15(c). It can be observed from the figure that the bending moment bearing capacity of the joint increases with increasing yield strength of the steel beam, but the initial stiffness is hardly affected by the varying f_{y1}. Because the elastic modulus of the steel beam (E) is minimally affected by the variation of the yield strength, the initial stiffness of the joint is thus not enhanced by an increase in the strength of the steel beam.

4.4. Effect of Strength of Steel Tubes (f_{y2}). Figure 15(d) shows the effect of the strength of the steel tubes (f_{y2}) on the M-θ relationship, with the variation of f_{y2} as 235, 345, 390, and 420 MPa. It can be seen from the figure that the bearing bending capacity at the failure stage of the composite joint increases with increasing f_{y2}, whereas there is only a slight effect on the initial stiffness of the joint.

4.5. Effect of Concrete Strength (f_{cu}). The effect of the strength of the concrete filled into the steel tubes (f_{cu}) on the M-θ relationship was also investigated. For this purpose, f_{cu} was varied as 30, 40, 60, and 80 MPa, as shown in Figure 15(e). An axial load level (n) of 0.6 was used for this parameter analysis to verify the excellent behavior of a CFDST column under heavy compressive loading. It was found that the composite joint exhibited good bending resistance under axial loading (load level $n = 0.6$), despite the C30 concrete filled into the steel tubes of the column. The ultimate bending capacity and initial stiffness of the joint were slightly enhanced with increasing concrete strength (f_{cu}).

4.6. Effect of Steel Ratio (α). To examine the effect of the steel ratio (α), a finite element analysis was performed in which α was varied as 0.109, 0.132, 0.194, and 0.237. The results are shown in Figure 15(f), from which it can be observed that the bending moment capacity and initial stiffness of the joint are significantly enhanced with increasing α of the CFDST column. The variation of α was achieved by varying the wall thickness of the outer steel tube. The increase of the tube wall thickness used to achieve a higher α increased the constraint on the filling concrete, as well as the flexural rigidity of the column. The steel ratio α was found to be the main impacting factor of the bending moment capacity and initial stiffness of the composite joint.

4.7. Effect of Beam-to-Column Linear Stiffness Ratio (k_i). Figure 15(g) shows the effect of the beam-to-column linear stiffness ratio (k_i) on the M-θ relationship. The variation of k_i was achieved by varying the length of the beam. It can be seen from the figure that the bending moment capacity and initial stiffness of the joint are obviously affected by k_i. However, the flexural capacity of the joint is significantly lower for a k_i value of 0.764 compared with other values. This is mainly because the relative beam-to-column rotation for $k_i = 0.764$ is larger for a given vertical displacement of the beam ends, resulting in an earlier damage of the beam. The beam-to-column linear stiffness ratio is a principal factor of the behavior of the composite joint, with a value of 0.5 being optimal.

4.8. Effect of Beam-to-Column Bending Capacity Ratio (k_m). The effect of the beam-to-column bending capacity ratio (k_m) on the M-θ relationship was examined by varying it as 0.436, 0.592, 0.664, and 0.721. As indicated by Figure 15(h), the bending moment capacity and initial stiffness of the joint significantly increase with increasing k_m, especially when k_m increases from 0.436 to 0.592. The variation of k_m was achieved by varying the size of the beam section. A beam-to-column bending capacity ratio of 0.6 is suggested for optimization of the composite joint. Nevertheless, in practical engineering applications, it is necessary to take both

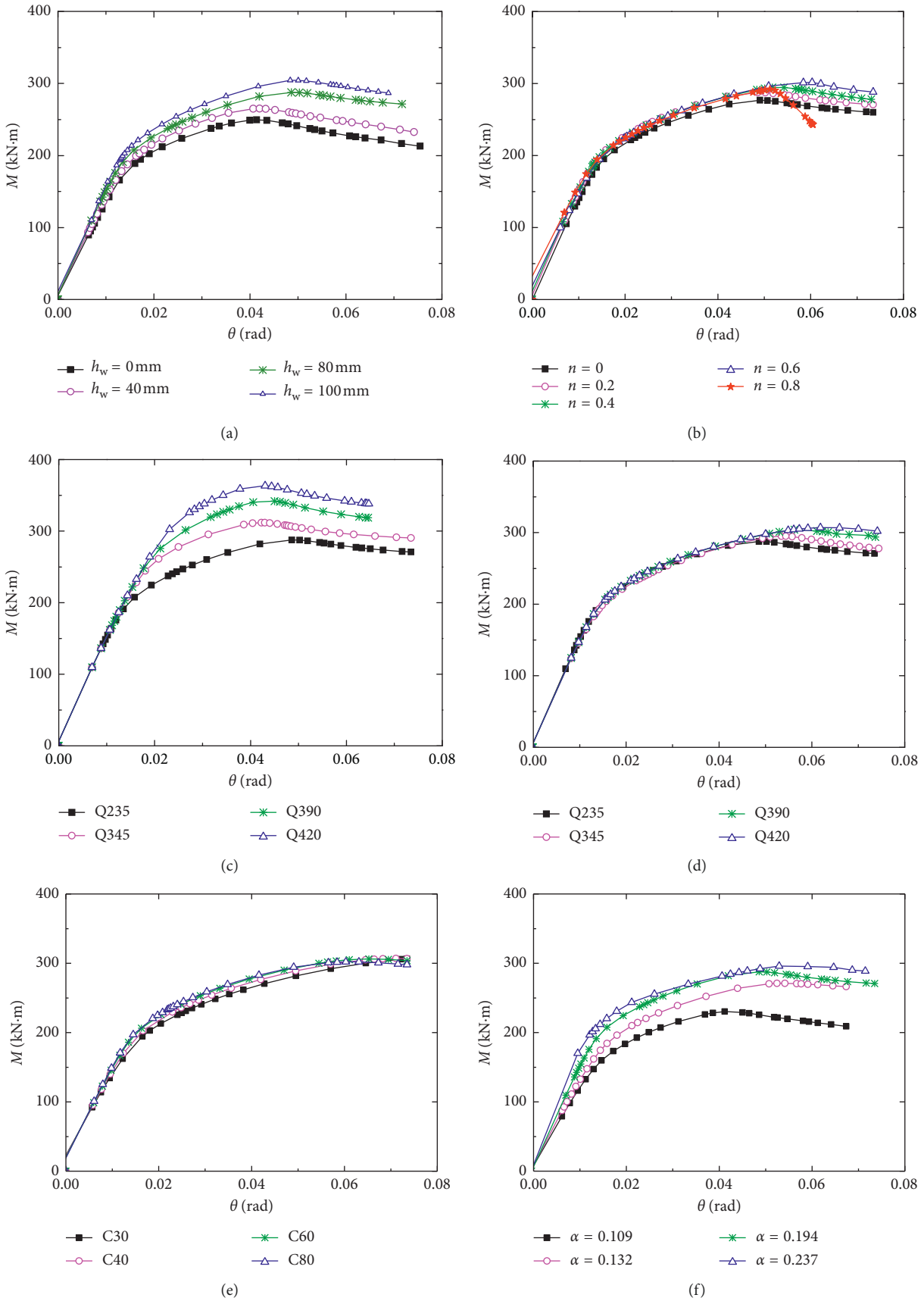

Figure 15: Continued.

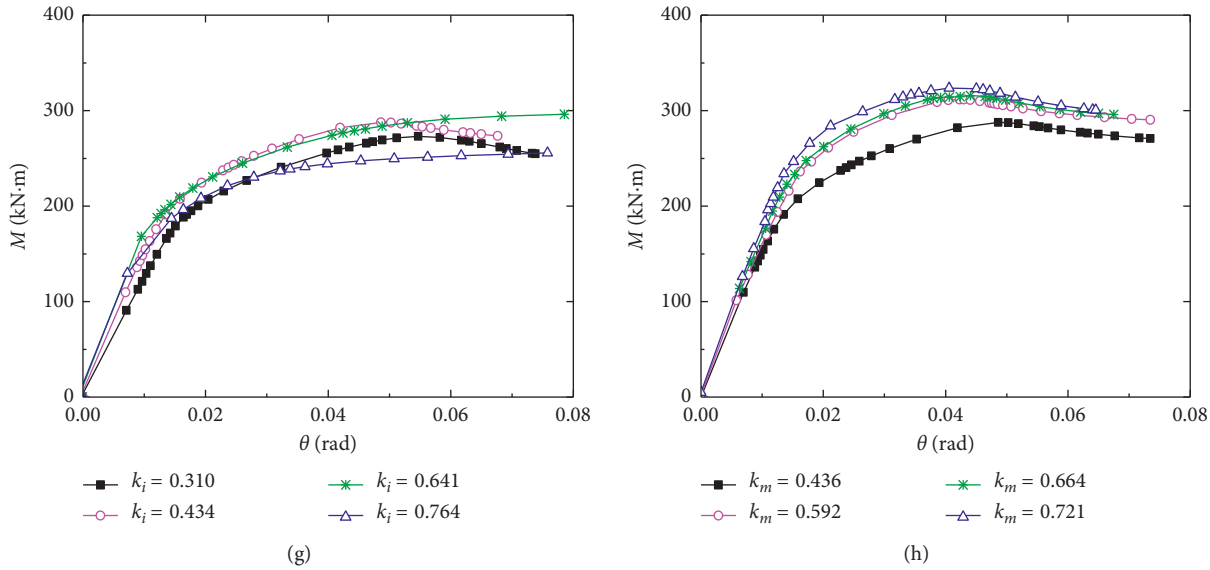

FIGURE 15: Effect of various parameters on the M-θ relationship of the CFDST column-beam joint. (a) Stiffened height (h_w). (b) Column axial load level (n). (c) Strength of beam steel (f_{y1}). (d) Strength of tube steel (f_{y2}). (e) Concrete strength (f_{cu}). (f) Steel ratio (α). (g) Beam-to-column linear stiffness ratio (k_i). (h) Beam-to-column bending capacity ratio (k_m).

economy and mechanical effectiveness into consideration in setting the beam-to-column bending moment ratio.

5. Conclusions

Based on the results of the experimental and numerical investigations of the steel-beam-CFDST-column joint in the present study, the following conclusions and design suggestions are presented:

(1) The plastic hinge of the joint under cyclic loading occurs at the beam ends. The extension of the vertical plate can be used to move the plastic hinge away from the face of the column to protect the core regions of the joints. The joint satisfies the design principles of "strong column, weak beam" and "strong joint, weak component" for seismic resistance.

(2) All the obtained moment-rotation hysteretic curves are plump, indicating an excellent energy dissipation capacity of the joint. The web anchorage plate with stiffening enhances the stiffness, bearing capacity, and energy dissipation capacity of the joint, enabling effective transfer of tensile stress from the beam segments to the column. The limit rotation of the joint reaches 0.05 rad in the failure state, satisfying the FEMA-350 ductility requirement of ≥0.03 rad for seismic resistance.

(3) The proposed FEA model of the steel-beam-CFDST-column composite joint is effective for predicting the behavior of the joint and can be used for further parametric analysis.

(4) Based on the results of parametric investigations, the stiffened height of the anchorage web plate and the strength of the steel beam significantly affect the bearing moment capacity of the joint, while the strengths of the concrete and steel tubes minimally affect that. The level of the axial load on the CFDST column moderately affects the bearing moment capacity of the joint. The joint still behaves well under a high axial load level of 0.6.

(5) The bending moment capacity and initial stiffness of the composite joint are significantly enhanced with increasing steel ratio of the CFDST column, beam-to-column bending capacity ratio, and beam-to-column linear stiffness. A beam-to-column bending capacity ratio of 0.6 and beam-to-column linear stiffness ratio of 0.5 are suggested for optimality of the composite joint.

Further theoretical investigation of the proposed mechanical model of the composite joint based on the conclusions of the present study is planned by the authors.

Data Availability

The data used to support the findings of this study are available from the corresponding author upon request.

Conflicts of Interest

The authors declare that there are no conflicts of interest related to this study.

Acknowledgments

This study was financially supported by the National Natural Science Foundation of China (NSFC) (Grant no. 51508028), the Natural Science Foundation of Shaanxi Province (Grant no. 2018JQ5119), the China Postdoctoral Science Foundation (Grant nos. 2014M562357 and 2015M580803), the

Special Fund for Basic Scientific Research of the Central Colleges (Grant nos. 300102288112 and 310828173402), and the Postdoctoral Research Project of Shaanxi Province.

References

[1] B. McKinley and L.-F. Boswell, "Behaviour of double skin composite construction," *Journal of Constructional Steel Research*, vol. 58, no. 10, pp. 1347–1359, 2002.

[2] L.-H. Han, H. Huang, and X.-L. Zhao, "Analytical behaviour of concrete-filled double skin steel tubular (CFDST) beam-columns under cyclic loading," *Thin-Walled Structure*, vol. 47, no. 6-7, pp. 668–680, 2009.

[3] L.-H. Han, W. Li, and R. Bjorhovde, "Developments and advanced applications of concrete-filled steel tubular (CFST) structures: members," *Journal of Constructional Steel Research*, vol. 100, pp. 211–228, 2014.

[4] Q.-Q. Liang, "Nonlinear analysis of circular double-skin concrete-filled steel tubular columns under axial compression," *Engineering Structure*, vol. 131, pp. 639–650, 2017.

[5] L.-H. Han and W. Li, "Seismic performance of CFST column to steel beam joint with RC slab: experiments," *Journal of Constructional Steel Research*, vol. 66, no. 11, pp. 1374–1386, 2010.

[6] W. Li and L.-H. Han, "Seismic performance of CFST column to steel beam joints with RC slab: analysis," *Journal of Constructional Steel Research*, vol. 67, no. 1, pp. 127–139, 2010.

[7] N. Jianguo, H. Yuan, Y. Weijian, and F. Jiansheng, "Seismic behavior of CFRSTC composite frames considering slab effects," *Journal of Constructional Steel Research*, vol. 68, no. 1, pp. 165–175, 2012.

[8] J.-F. Wang and B.-F. Spencer, "Experimental and analytical behavior of blind bolted moment connections," *Journal of Constructional Steel Research*, vol. 82, no. 1, pp. 33–47, 2013.

[9] L.-P. Kang, R.-T. Leon, and X.-L. Lu, "Shear strength analyses of internal diaphragm connections to CFT columns," *Steel and Composite Structures*, vol. 18, no. 5, pp. 1083–1101, 2015.

[10] O. Rezaifar and A. Younesi, "Finite element study the seismic behavior of connection to replace the continuity plates in (NFT/CFT) steel columns," *Steel and Composite Structures*, vol. 21, no. 1, pp. 73–91, 2016.

[11] Z. Tao, W. Li, B.-L. Shi, and L. H. Han, "Behaviour of bolted end-plate connections to concrete-filled steel columns," *Journal of Constructional Steel Research*, vol. 134, pp. 194–208, 2017.

[12] J.-C. Liu, Y.-L. Yang, J.-P. Liu, and X. Zhou, "Experimental investigation of special-shaped concrete-filled steel tubular column to steel beam connections under cyclic loading," *Engineering Structures*, vol. 151, pp. 68–84, 2017.

[13] Y.-F. Zhang, J.-H. Zhao, and C.-S. Cai, "Seismic behavior of ring beam joints between concrete-filled twin steel tubes columns and reinforced concrete beams," *Engineering Structures*, vol. 39, pp. 1–10, 2012.

[14] D.-F. Zhang, Y.-F. Zhang, and J.-H. Zhao, "Finite element analysis on the ring beam joint with discontinuous outer tube between composite CFST and RC beams," *Building Structures*, vol. 43, no. 5, pp. 39–44, 2013, in Chinese.

[15] Y.-F. Zhang, D.-F. Zhang, and J.-H. Zhao, "Experimental study on seismic behavior of the connection between composite CFST column and H-shape steel beam," *Journal of Building Structure*, vol. 34, no. 9, pp. 40–48, 2013, in Chinese.

[16] GB 50936-2014, *Technical Code for Concrete Filled Steel Tubular Structures*, China Architecture & Industry Press, Beijing, China, 2014, in Chinese.

[17] JGJ/T 101-2015, *Specification for Seismic Test of Buildings*, China Architecture & Building Press, Beijing, China, 2015, in Chinese.

[18] GB/T 228.1-2010, *Metallic Materials-Tensile Testing-Part I: Method of Test at Room Temperature*, China Standard Press, Beijing, China, 2010, in Chinese.

[19] N. Abdel-Rahman and K. Sivakumaran, "Material properties models for analysis of cold-formed steel members," *Journal of Structural Engineering*, vol. 123, no. 9, pp. 1135–1143, 1997.

[20] L.-H. Han, Z. Tao, and W.-D. Wang, *Advanced Composite and Mixed Structure-Testing, Theory and Design Approach*, China Science Press, Beijing, China, 2009, in Chinese.

[21] J. Lubliner, J. Oliver, S. Oller, and E. Oñate, "A plastic-damage model for concrete," *International Journal of Solids and Structures*, vol. 25, no. 3, pp. 299–326, 1989.

[22] J. Lee and G. Fenves, "Plastic-damage model for cyclic loading of concrete structures," *Journal of Engineering Mechanics*, vol. 124, no. 8, pp. 892–900, 1998.

[23] L.-H. Han, G.-H. Yao, and Z. Tao, "Performance of concrete-filled thin-walled steel tubes under pure torsion," *Thin-Walled Structure*, vol. 45, no. 1, pp. 24–36, 2007.

[24] GB 50011-2010, *Code for Seismic Design of Buildings*, China Architecture & Industry Press, Beijing, China, 2010, in Chinese.

[25] J. Zhang, Q.-Y. Wang, S.-Y. Hu et al., "Parameters verification of concrete damaged plastic model of ABAQUS," *Building Structure*, vol. 38, no. 8, pp. 127–130, 2008, in Chinese.

[26] S. Schneider, "Axially loaded concrete-filled steel tubes," *Journal of Structural Engineering*, vol. 124, no. 10, pp. 1125–1138, 1998.

[27] C. Roeder, B. Cameron, and C. Brown, "Composite action in concrete filled tubes," *Journal of Structural Engineering*, vol. 125, no. 5, pp. 477–484, 1999.

[28] FEMA-350, *Recommended Seismic Design Moment-Frame Buildings*, Federal Emergency Management Agency, Washington, DC, USA, 2000.

[29] Y.-F. Zhang, J.-H. Zhao, and Y.-Y. Liu, "Calculation of compressive bearing capacity of concrete-filled twin steel tubes based on twin shear unified strength theory," *Mechanics in Engineering*, vol. 34, no. 3, pp. 36–42, 2012, in Chinese.

[30] CECS 159: 2004, *Technical Specification for Structures With Concrete-Filled Rectangular Steel Tube Members*, China Planning Press, Beijing, China, 2004, in Chinese.